

# Strain analysis from shape preferred orientation in magmatic rocks

ANGEL FERNANDEZ

Fernandez, A. 1988 12 30: Strain analysis from shape preferred orientation in magmatic rocks. *Bulletin of the Geological Institutions of the University of Uppsala*, N.S., Vol. 14, pp. 61–67. Uppsala. ISSN 0302-2749.

A close relationship between fabric development and strain allows the preferred orientation of minerals to be used for the analysis of strain in magmatic rocks. In fabrics derived from coaxial or slightly rotational strain histories, the eigenvalues of the weighted orientation tensor obtained from fabric data are related to the principal quadratic extensions of the finite strain ellipsoid by a power law. This relationship allows petrofabric data to constrain the strain symmetry parameters as well as the strain intensity parameters. This method is applied to the study of the intrusion of the Gelles granite (French Massif Central) for which strain symmetry maps and strain intensity maps are presented.

*A. Fernandez. Department des Sciences de la Terre, OPGC et U.A. No 10 CNRS, 5 rue Kessler, 63038 Clermont-Ferrand Cedex, France. Received 2nd June 1987, Revision received 25th January 1988.*

*Present address: Laboratoire de Géologie Régionale et Appliquée, Université de Limoges. 123 rue Albert Thomas. 87060 Limoges, France.*

## Introduction

Many different methods are currently used for strain analysis in structural studies. However, few of these are appropriate for analysing intrusion strains because they are based on deformation of passive markers such as oolites (Cloos, 1947), reduction spots (Ramsay, 1967), quartz-grains (Flinn, 1956; Stauffer, 1967), or enclaves (Holder, 1979). Methods based on petrofabric analysis are more appropriate for studying magmatic rocks. March (1932) has shown, theoretically, that a system containing linear (L) or planar (S) passive markers with initially random orientation will develop a preferred orientation related respectively to the finite strain ellipsoid and the inverse ellipsoid by:

$$D = \Delta r^3 \quad (\text{for L markers}) \quad (1)$$

and

$$D = \Delta r^3 \quad (\text{for S markers}) \quad (2)$$

where  $D$  is the orientation density of markers axes in any direction (relative to a uniform distribution),  $\Delta$  is the dilation,  $r$  is the length of the vector radius of the finite strain ellipsoid in the same direction, and  $r$  is the length of the vector radius of the inverse ellipsoid. Note that the density solution for linear markers (eq. 1) is the inverse of that for planar markers (eq. 2). This is because the orientation is

defined by the direction and azimuth of the elements themselves in the first case, and by the poles to planar elements in the second case. If no dilation takes place ( $\Delta = 1$ ) and if the orientation density is given, as usual, in multiples of the uniform distribution, the following relationships hold:

$$a) D = r^3 \quad \text{and} \quad b) D = r^3 \quad (3)$$

for linear and planar markers respectively.

Many petrologists have applied this model to evaluate strain from preferred orientation in metamorphic rocks (Oertel, 1974; Tullis & Wood, 1975) and have compared the results with those obtained using other methods. Other authors have tested the agreement between March's model and experimental data (Means & Paterson, 1966; Tullis, 1971, 1976). The differences suggest that March's model can be applied to systems containing markers with aspect ratios that are high ("needle-like") or very low ("flakes"), provided that the finite strain has not been too high. However, the application of March's model to magmatic systems has been limited because the crystals behave as rigid markers, and because their aspect ratios are seldom "needle-" or "flake-like". Here I present a generalization of March's model (see also Fernandez, 1981) and discuss the use of orientation data for magmatic crystals in a "quantitative intrusion-strain analysis" (Q. I.S.A.).

### Preferred orientation and strain

The strain path defining the evolution of any portion of a magma through its intrusion history is potentially very complex. The reconstitution of such strain paths is most likely impossible, owing to the viscous behavior of the magma and its consequent inability to record any feature related to progressive strain. Nevertheless, the final preferred orientation is closely related to at least the late strain history. Willis (1977) has proposed a kinematic model which predicts the preferred orientation developed by any population of markers when the strain history is specified by a macroscopic strain-rate tensor. Unfortunately, it is impossible to solve the inverse problem applying Willis' model. Mathematical relationships between orientation density and finite strain parameters (derived from particular strain regimes) are better adapted to evaluate finite strain from orientation data.

Before presentation of some mathematical relationships which may be used for intrusion-strain analysis it is appropriate to discuss three factors which have a noticeable effect on preferred orientation: the shape of the markers, the strain regime, and the strain intensity.

#### *Effect of the shapes of markers*

Marker shape has a noticeable effect on preferred orientation intensity. This effect is well illustrated by a two-dimensional computer simulation of preferred orientation developed by two families of markers under the effect of a coaxial flattening (Fig. 1). The rotation of a two-dimensional marker with aspect ratio  $n$ , during a coaxial strain, is given by (Fernandez, 1984):

$$\frac{\tan \theta'}{\tan \theta} = \left( \frac{\lambda_2}{\lambda_1} \right)^\alpha \quad (4)$$

where  $\theta$  and  $\theta'$  are the angles between the major axis of the marker and the lengthening axis of the strain before and after applying the strain, respectively,  $\lambda_1$  and  $\lambda_2$  are the conventional principal quadratic extensions, and  $\alpha$  is a shape parameter related to  $n$  by:

$$\alpha = (n^2 - 1) / (n^2 + 1).$$

Equation (4) has been applied to the different markers of the two populations in the computer simulation of figure 1. Note the conspicuous difference between the intensities of the preferred orientation

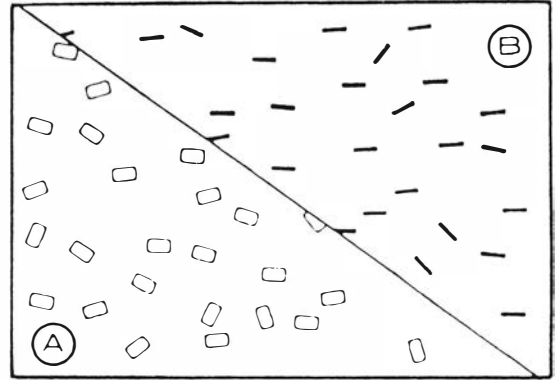


Figure 1. - Computer simulation of the preferred orientation developed by two different populations of markers under the effect of the same finite strain (in both cases,  $\lambda_1/\lambda_2 = 100$ ). Aspect ratio of the markers: A,  $n = 1.75$ ; B,  $n = 6$ .

shown by the two families of markers. Similar behaviour can be expected in three-dimensional systems. This result shows that, for a given finite strain, different families of markers will develop distinct subfabric ellipsoids which depend strongly on the shapes of the markers.

#### *Strain fields and strain regimes*

To study the rotation of a rigid marker embedded in a viscous matrix in a given strain field, it is useful to consider two, distinct, coordinate systems:

- the Lagrangian marker system defined by the axes  $X_1, X_2, X_3$  with its origin 0 (at the center of the marker, and moving with it);
- the Eulerian external system (or observer system) defined by the axes  $\chi_1, \chi_2, \chi_3$ , and the origin 0 (fixed also at the center of the marker) (Fig. 2).

A macroscopic strain field can be characterized by a strain-rate tensor  $\dot{\epsilon}(t)$ , which, in the more general case, varies with time. Then, any particular strain history may be described, specifying  $\dot{\epsilon}(t)$ . Using the well known separation into symmetric and asymmetric parts, this tensor may be written:

$$\dot{\epsilon}(t) = \dot{\epsilon}(t) + \dot{\rho}(t) \quad (5)$$

where  $\dot{\epsilon}(t)$  represents the pure strain-rate and  $\dot{\rho}(t)$  the rigid-body rotation rate. If  $\dot{T}(t)$  is this same tensor referred to the marker system, we may write:

$$\dot{T}(t) = \dot{E}(t) + \dot{R}(t) \quad (6)$$

and in terms of the tensor components:

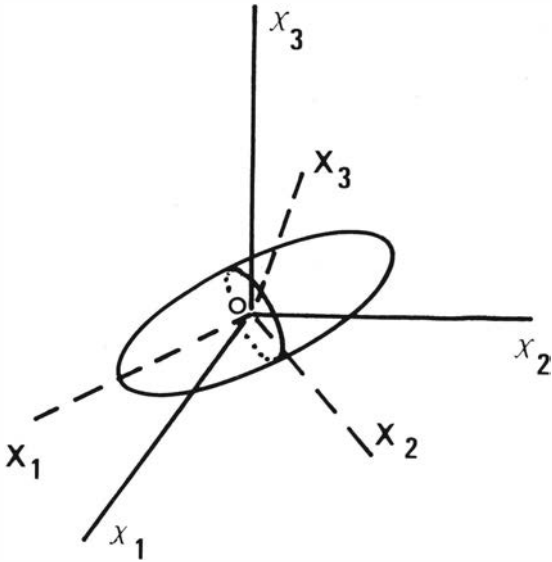


Figure 2. – Reference coordinate systems:  $X_1$ ,  $X_2$ , and  $X_3$ , are the axes of the marker system;  $\chi_1$ ,  $\chi_2$ , and  $\chi_3$ , are the axes of the observer system. The common origin is 0.

$$\dot{T}(t) = \begin{bmatrix} \dot{\epsilon}_{11} & \dot{\epsilon}_{12} & \dot{\epsilon}_{13} \\ \dot{\epsilon}_{21} & \dot{\epsilon}_{22} & \dot{\epsilon}_{23} \\ \dot{\epsilon}_{31} & \dot{\epsilon}_{32} & \dot{\epsilon}_{33} \end{bmatrix} + \begin{bmatrix} 0 & \dot{r}_3 & -\dot{r}_2 \\ -\dot{r}_3 & 0 & \dot{r}_1 \\ \dot{r}_2 & -\dot{r}_1 & 0 \end{bmatrix} \quad (7)$$

As the marker rotates in the strain field, the components of  $\dot{T}(t)$  vary with time, even when the components of  $\dot{\tau}(t)$  do not vary. In this latter case, the tensor will be denoted  $\dot{\tau}$ .

We may define the strain regime as a macroscopic strain field which is invariable with time and can be described by a simple form of the tensor  $\dot{\tau}$ .

*Effect of strain regime*

The strain regime has a definite effect on fabric symmetry. We have already seen that a given coaxial strain results in different families of markers developing preferred orientations characterized by distinct subfabric ellipsoids. In addition, the principal axes of these subfabric ellipsoids are coaxial; that is, the bulk fabric is homoaxial. Another characteristic of fabrics developed under coaxial strain regimes is that the fabric symmetry is always high (axial or orthorhombic). This is supported by computer simulation of fabrics developed under plane, coaxial strain (Reed & Tryggvason, 1974; Blanchard *et al.*, 1979).

The effect of non-coaxial strain regimes is more complex. If a system undergoes a non-coaxial strain,

each population of markers will develop a preferred orientation characterized by its own subfabric ellipsoid, as in the preceding case. However, an important difference appears in fabric symmetry. The different subfabric ellipsoids will rotate at different rates (Fernandez, 1982). Thus, if the markers of a given family are not the same shape, the resulting subfabric is monoclinic and, if the system contains two or more populations of markers, the resulting bulk fabric is heteroaxial. These theoretical conclusions have been verified experimentally (Fernandez *et al.*, 1983).

*Effect of strain intensity*

March's equations (3, a and b) quantitatively relate preferred orientation to strain intensity in the case of systems containing L or S, passive markers. The effect of strain on systems containing three-dimensional, rigid, axial markers has been studied by several authors. Solutions have been given for simple shear (Jeffery, 1922), for plane coaxial strain (Gay, 1968), and for uniaxial flattening (Tullis, 1971, 1976; Debat *et al.*, 1975). The general case of orthorhombic strain is presented here.

Willis (1977) has proposed a kinematic model of preferred orientation development. The basis of this model is that the rotation ratio of an ellipsoidal marker, around its own axes, varies linearly with the applied strain-rate tensor  $\dot{T}(t)$ . Willis' model predicts that, whatever the strain history, the preferred orientation developed by a system containing axial markers of identical shape, will always be described by a fabric ellipsoid, provided that the strain is homogeneous. The rotation rates ( $\omega_1$ ,  $\omega_2$ , and  $\omega_3$ ) of an axial marker around its own axes ( $X_1$ ,  $X_2$ , and  $X_3$ ) are a function of the strain-rate tensor and of the shape of the markers. If  $n$  is the aspect ratio of a three-dimensional axial marker, we can define a three-dimensional shape parameter  $K$  in the same way as defined earlier; that is,  $K = (n^2 - 1) / (n^2 + 1)$ . Using the notation of equation (7) for the tensor components, Willis' equations (op. cit.) are given by:

$$\begin{aligned} \omega_1 &= \dot{r}_1 \\ \omega_2 &= -K\dot{\epsilon}_{31} + \dot{r}_2 \end{aligned} \quad (8)$$

and

$$\omega_3 = K\dot{\epsilon}_{12} + \dot{r}_3$$

where  $K$  is the shape parameter as defined before.

I will now consider the tensor  $\dot{\tau}$ , corresponding to the most general coaxial strain regime. As this ten-

isor is symmetric, referred to marker system of axes, we have:

$$\dot{T}(t) = \dot{E}(t) \tag{9}$$

since the components of  $\dot{R}(t)$  are zero. Thus, the relationships in equation (8) reduce to:

$$\begin{aligned} \omega_1 &= 0 \\ \omega_2 &= -K\dot{\epsilon}_{31} \end{aligned} \tag{10}$$

and

$$\omega_3 = K\dot{\epsilon}_{12}$$

Note that  $K$  affects only the pure strain components, and that the rotation induced by the tensor  $\dot{E}(t)$  on an axial marker with shape parameter  $K$ , is the same as the rotation induced in a needle-like marker by a tensor  $K\dot{E}(t)$ . Thus, every finite strain ellipsoid produced by the action of the tensor  $\dot{E}(t)$ , acting during an arbitrary time  $t$  (on markers with shape parameter  $K$ ), has a corresponding fabric ellipsoid defined by the tensor  $K\dot{E}(t)$ , acting during the same period (on needle-like markers). At the same time, the tensor  $K\dot{E}(t)$  corresponds to a macroscopic strain-rate tensor  $K\dot{\epsilon}$ . As the principal components of the strain-rate tensor are given by  $\dot{\epsilon}_1 = d\epsilon_1/dt$ ,  $\dot{\epsilon}_2 = d\epsilon_2/dt$  . . . etc., integrating over time interval  $(t)$ , required to produce a fictive, finite strain ellipsoid defined by the principal natural strain  $\epsilon_1$ ,  $\epsilon_2$ , and  $\epsilon_3$ , we obtain the fabric ellipsoid corresponding to this imaginary finite strain. A finite strain ellipsoid, defined by  $\epsilon_1$ ,  $\epsilon_2$ , and  $\epsilon_3$ , will correspond to a fabric ellipsoid defined by  $K\epsilon_1$ ,  $K\epsilon_2$ , and  $K\epsilon_3$ . In other words, a coaxial strain, characterized by a finite strain ellipsoid having principal quadratic extensions  $\lambda_1$ ,  $\lambda_2$ , and  $\lambda_3$ , acting on a system containing markers of shape parameter  $K$ , produces a preferred orientation characterized by a fabric ellipsoid with principal quadratic semiaxes given by:

$$\Lambda_1 = \lambda_1^K \quad \Lambda_2 = \lambda_2^K \quad \text{and} \quad \Lambda_3 = \lambda_3^K \tag{11}$$

for prolate markers, and

$$\Lambda_1 = \lambda_3^K \quad \Lambda_2 = \lambda_2^K \quad \text{and} \quad \Lambda_3 = \lambda_1^K \tag{12}$$

for oblate markers.

Note that the density maximum  $D_M$  is related to strain by:

$$D_M = \lambda_1^{3K/2} \quad (\text{for prolate markers}) \tag{13}$$

and

$$D_M = \lambda_3^{3K/2} \quad (\text{for oblate markers}) \tag{14}$$

because relationships equivalent to (3) relate the orientation density to the vector radius of the fabric ellipsoid. Relationships (11) to (14) constitute the basis of the Q.I.S.A.

### Strain analysis from orientation data

The characteristics of the orientation distribution corresponding to any set of directional data can be obtained by statistical methods or by calculating an orientation tensor (Scheidegger, 1965; Cobbold & Gapais, 1979). The fabric axes may be obtained directly from a weighted orientation tensor ( $W$ . O.T.) (Cobbold & Gapais, 1979) defined by:

$$W = \frac{3}{N} \begin{bmatrix} \sum r_i^2 x_i^2 & \sum r_i^2 x_i y_i & \sum r_i^2 x_i z_i \\ \sum r_i^2 y_i x_i & \sum r_i^2 y_i^2 & \sum r_i^2 y_i z_i \\ \sum r_i^2 z_i x_i & \sum r_i^2 z_i y_i & \sum r_i^2 z_i^2 \end{bmatrix} \tag{15}$$

where:

- $x_i, y_i, z_i$ , are the direction cosines of the  $i$  datum referred respectively to the axes  $\chi_1, \chi_2$ , and  $\chi_3$ ;
- $r_i$  is the cubic root of the orientation density along direction  $i$ ;
- and  $N$  is the total number of data.

The eigenvalues  $W_1, W_2$ , and  $W_3$ , of the  $W$ .O.T. are respectively the best estimates of the quadratic semiaxes ( $\Lambda_1, \Lambda_2$ , and  $\Lambda_3$ ) of the fabric ellipsoid, that is:

$$W_1 \approx \Lambda_1 \quad W_2 \approx \Lambda_2 \quad \text{and} \quad W_3 \approx \Lambda_3 \tag{16}$$

Relationships (16), together with (11) to (14), allow the derivation of strain values from orientation data.

Theoretically, these relationships apply only to fabrics derived through coaxial strain. However, they can also be used when the strain is characterized by a slight to moderate rotational component. In practice, coaxial or slightly non-coaxial strain histories are recognized through the high symmetry of the subfabrics (orthorhombic or axial) and the homoaxial character of the bulk fabric. If the non-coaxial part of the strain history is significant, noticeable differences appear in the orientations of the first eigenvectors of the different sub-fabric ellipsoids.

The normal steps in performing Q.I.S.A. are

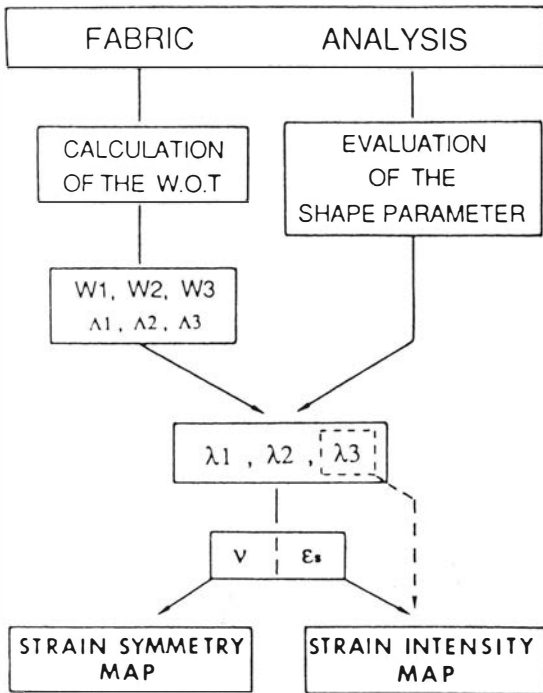


Figure 3. — The steps usually followed in intrusion-strain analysis.

shown in Figure 3. The  $\nu$  and  $\epsilon_s$  parameters are respectively "Lode's ratio" (a symmetry parameter) and "natural octahedral strain" (an intensity parameter). Calculating these parameters from orientation data obtained at different points in a pluton allows construction of strain symmetry and strain intensity maps. Note that, using relationships (13) and (14), it is possible also to obtain valuable information on the strain parameters  $\lambda_1$  or  $\lambda_3$ , depending on the shapes of the markers. Strain intensity maps constructed from  $\lambda_3$  data may be specially useful for studying the upper levels of diapiric structures, where strains characteristic of the flattening field can be expected.

### Application to plutonic massifs

An analysis of the Gelles granite, in the French Massif Central (F.M.C.), is offered as an example of application of the method. The Gelles granite crops out in the central part of the F.M.C., west of the volcanic "Chain of Puys". The main facies is a grey coarse-grained, porphyritic granite containing 13–15 vol. % K-feldspar megacrysts, 3 to 5 cm long. The general shape of the massif is elliptical (11

× 6 km) with its major axis oriented ENE-SSW (Fig. 4). Two parallel faults affect the massif in the western zone. Internal structures in the granite are indicated by the preferred orientation of the feldspar megacrysts which, in the outer zones of the massif, tend to be oriented parallel to the contacts.

The granite is surrounded by gneisses and micaschists, except on its northern side where cordierite-rich migmatites occur. Four distinct deformation phases has been recognized in the gneisses and micaschists (Fernandez & Tempier, 1977). The last phase (P4) is characterized by large, open, cylindrical folds with vertical axial planes and axes striking S 20 E to N-S. The P4 axes plunge gently northwards in the north of the massif, and southwards in the South (Fig. 4), suggesting that they have been tilted by the intrusion. Both the external plunging of the P4 axes and the internal structure of the granite suggest that the Gelles granite is a posttectonic diapiric intrusion.

The internal structure of the pluton has been studied using feldspar megacryst subfabric analysis. Thirty four outcrops were studied, 30 east of the Prondines fault and, because outcrops are poor and few, only 4 to the west. At each outcrop 100 to 120 measurements were made of the orientation of the (010) feldspar face, to ensure statistical significance. Measurements can easily be made if differential wea-

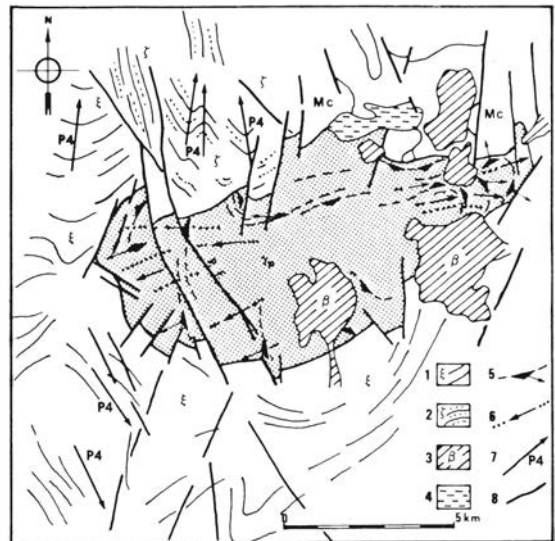


Figure 4. — Structural map of the Gelles granite. Key: 1 — mica schists; 2 — gneisses; 3 — basaltic cover; 4 — rhyolitic tuffs; 5 — apparent flow planes with associated  $\lambda_1$  direction (arrow); 6 — apparent flow lines (arrow: mean  $\lambda_1$  direction); 7 — fold axes of the phase P4; 8 — faults; P.F. — Prondines fault;  $\gamma_p$  porphyritic granite; Mc — cordierite-rich migmatites.

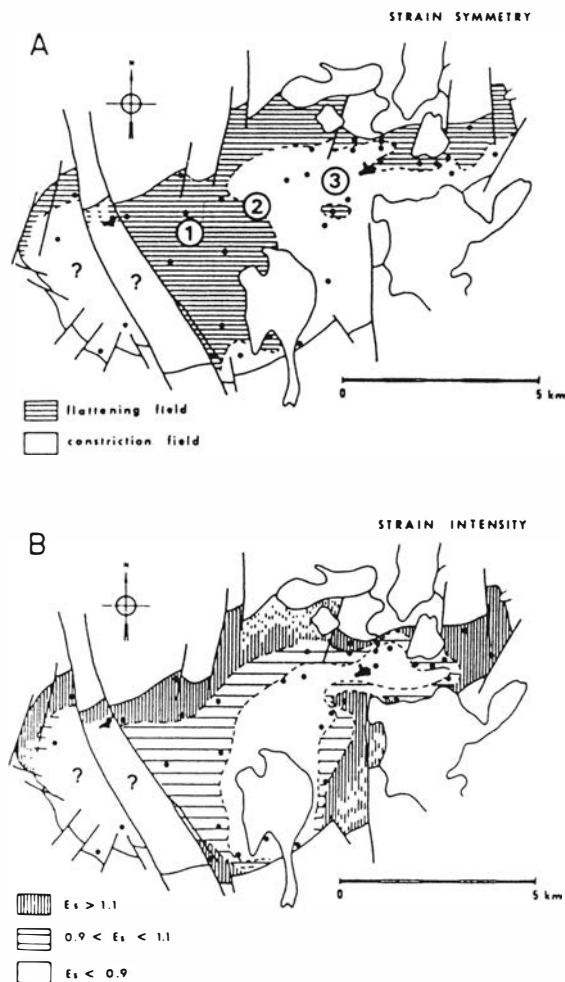


Figure 5. — Strain maps of the Gelles granite. A — Strain symmetry map: 1, flattening field ( $v > 0$ ); 2,  $v = 0$ ; 3, constriction field ( $v < 0$ ). B — Strain intensity map. The black dots locate the studied outcrops.

thering has caused feldspars to stand out of their matrix, or if the outcrops have rough surfaces.

The mean shape parameter  $K$  was evaluated from 20 feldspar megacrysts extracted from weathered outcrops. For each crystal, the aspect ratio ( $n$ ) was calculated by dividing the width of the crystal (along the  $b$  crystallographic axis) by the geometrical mean of the length (along the  $c$  axis and an axis  $a'$  perpendicular to the plane  $bc$ ). The strain parameters  $v$  and  $\epsilon_s$  were calculated from the field data following the steps outlined in Figure 3, and using a computer routine. These parameters were used to draw strain symmetry (Fig. 5A) and strain intensity maps (Fig. 5B). Data from the western

part of the pluton are insufficient to characterize the strain pattern there.

The symmetry map (Fig. 5A) reveals that a large central part of the pluton, is characterized by constriction fabrics ( $v < 0$ ). According to the experimental results of Dixon (1975) and finite-element models of diapiric ridges (van Berkel, this volume), the symmetry pattern observed in the Gelles granite indicates that the pluton has been eroded to an intermediate or deep structural level, below the "neutral surface" corresponding to the change in the symmetry field. The strain intensity map reveals higher strains near the contacts and lower values toward the center of the pluton. Both symmetry and strain intensity maps agree well with experimental and theoretical models of diapiric structures and suggest that the Gelles granite is a posttectonic, diapiric intrusion, exposed at a structural level below the neutral surface.

## Discussion and conclusions

Theoretical analysis shows that, in petrofabrics with high symmetry, the quadratic semi-axes of the fabric ellipsoid are related to the conventional quadratic extensions of the finite strain ellipsoid by a simple power law. The calculation of a weighted orientation tensor from orientation data allows evaluation of the principal quadratic semi-axes of the fabric ellipsoid. The value of these fabric axes can be used to calculate various strain parameters. An example of the application of this method, at the pluton scale, is illustrated by strain symmetry and strain intensity maps of the Gelles granite.

The method outlined here probably underestimates the true finite strain. Two factors may contribute to this effect: an insufficient strain memory of the magma at the beginning of the intrusion history, and an increase in the mutual interference of the crystals as crystallization advances (e.g. Ildefonse & Fernandez, this volume). The strain parameters calculated from preferred orientation data in magmatic rocks should therefore be considered as indicating minimum finite strains.

## REFERENCES

- Berkel, J.T. van. 1988 (this volume): Kinematic evaluation of a finite-element model of a diapiric ridge. *Bull. Geol. Inst. Univ. Uppsala, N.S. 14*, 111–114.  
 Blanchard, J.Ph., Boyer, P. & Gagny, Cl. 1979: Un nouveau critère de sens de mise en place dans une caisse filonienne: le "pincement" des minéraux aux épontes. *Tectonophysics 53*, 1–25.

- Cloos, E. 1947: Oolite deformation in the South Mountain fold, Maryland. *Geol. Soc. Am. Bull.* 58, 843–918.
- Cobbold, P. & Gapais, D. 1979: Specification of fabric shapes using an eigenvalue method: Discussion. *Geol. Soc. Am. Bull.* 90, 310–312.
- Debat, P., Sirieys, P., Deramont, J. & Soula, J.C. 1975: Paléodéformations d'un massif orthogneissique (Massif des Cammazes, Montagne Noire occidentale, France). *Tectonophysics* 28, 159–183.
- Dixon, J.M. 1975: Finite strain and progressive deformation in models of diapiric structures. *Tectonophysics* 28, 89–124.
- Fernandez, A. & Tempier, P. 1977: Mise en place, fabrique mésostructurale et rapports structuraux du granite de Gelles avec l'enveloppe métamorphique. *Bull. B.R.G.M.*, (2), IV/4, 357–366.
- Fernandez, A. 1981: Une généralisation du modèle de March applicable à l'analyse des orientations préférentielles de forme issues de la déformation coaxiale dans les roches éruptives. *C.R. Acad. Sc. Paris* 294, Ser. 2, 1091–1094.
- Fernandez, A. 1982: Signification des symétries de fabrique monocliniques dans les roches magmatiques. *C.R. Acad. Sc. Paris* 294, Ser. 2, 995–998.
- Fernandez, A., Feybesse, J.L., & Mezure, J.F. 1983: Theoretical and experimental study of fabric developed by different shaped markers in two-dimensional simple shear. *Bull. Soc. géol. France* (7), 25/3, 319–326.
- Fernandez, A. 1984: *Etude théorique et expérimentale du développement de la fabrique dans les roches magmatiques. Application à l'étude structurale des granitoides.* Thèse ès Sci. Univ. Clermont II. 252 p.
- Flinn, D. 1956: Deformation of the Funzie conglomerate, Fetlar, Shetland. *J. Geol.* 64, 480–505.
- Gay, N.C. 1968: The motion of rigid particles embedded in a viscous fluid during pure shear deformation of the fluid. *Tectonophysics* 5, 81–88.
- Holder, M.T. 1979: An emplacement mechanism for post-tectonic granites and its implications for their geochemical features. In Atherton, M.P. & Tarney, J. Ed.: *Origin of granite batholiths. Geochemical evidence.* Shiva Publishers, Exeter, 116–128.
- Ildelfonse, B. & Fernandez, A. 1988 (this volume): Influence of the concentration of rigid markers in a viscous medium on the production of preferred orientations. An experimental contribution. *Bull. Geol. Inst. Univ. Uppsala. N.S. 14*, 55–60.
- Jeffery, J.B. 1922: The motion of ellipsoidal particles immersed in a viscous fluid. *Proc. Roy. Soc. London, Ser. A*, 102, 161–179.
- March, A. 1932: Mathematische Theorie der Regelung nach der Korngestalt bei affiner Deformation. *Zeitschr. f. Kristallogr.* 81, 285–297.
- Means, W.D. & Paterson, M.S. 1966: Experiments on preferred orientation of platy minerals. *Contr. Mineral. Petrol.* 13, 108–133.
- Oertel, G. 1974: Finite strain measurements: a comparison of methods. *Trans. Am. Geophys. Union* 55/7, 695.
- Ramsay, J.G. 1967: *Folding and fracturing of rocks.* McGraw-Hill, New York. 568 pp.
- Reed, L.J. & Tryggvason, E. 1974: Preferred orientation of rigid particles in a viscous fluid matrix deformed by pure shear and simple shear strain. *Tectonophysics* 24, 85–98.
- Scheidegger, A.E. 1965: On the statistics of the orientation of bedding planes, grain axes, and similar sedimentological data. *U.S. Geol. Surv. Prof. Paper* 525-C, 164–167.
- Stauffer, M.R. 1967: Tectonic strain in some volcanic, sedimentary, and intrusive rocks near Canberra, Australia, a comparative study in deformation fabrics. *N. Z. J. Geol. Geophys.* 10, 1079–1108.
- Tullis, T.E. 1971: *Experimental development of preferred orientation of mica during recrystallization.* Ph.D. Thesis. Univ. California, Los Angeles, 262 p.
- Tullis, T.E. 1976: Experiments on the origin of slaty cleavage and schistosity. *Geol. Soc. Am. Bull.* 87, 745–753.
- Tullis, T.E. & Wood, D.S. 1975: Correlation of finite strain from both reduction bodies and preferred orientation of mica in slates from Wales. *Geol. Soc. Am. Bull.* 86, 632–638.
- Willis, D.G. 1977: A kinematic model of preferred orientation. *Geol. Soc. Am. Bull.* 88, 883–894.